THE ASTROPHYSICAL JOURNAL, 435:55–65, 1994 November 1

EMISSION-LINE PROFILES FROM A RELATIVISTIC ACCRETION DISK AND THE ROLE OF ITS MULTIPLE IMAGES

G. BAO,[1,2] P. HADRAVA,[3] AND E. ØSTGAARD[1,4]
Received 1993 December 15; accepted 1994 May 3

ABSTRACT

Emission lines from a relativistic accretion disk around a black hole are studied by using quasi-analytic solutions of photon geodesics. Unlike the previous approaches, in this paper, the effects of the multiple images of the disk are considered, i.e., the contribution to the line profiles of the photons from the upper side of the disk as well as that from the back side with the photon trajectories crossing the plane of the disk. Different from the Newtonian case, the gravitational bending of light and the central black hole makes the photons visible to the observer at infinity. Because they are near the black hole, the trajectories of these higher order–image photons have more probability of penetrating the disk plane below the inner edge of the optically thick accreting matter and to reach us. For an optically thin disk, all the higher order–image photons can be observed; the two sides of a disk with an edge-on geometry should, in principle, make equal contribution to the observed flux. Therefore, the contribution to the line intensity from the back side of an accretion disk for a highly inclined system is as important as that from its upper side.

Profiles with various free parameters are shown. Lines of higher order–image photons contrast both in strength and in shape from those of zero order. Higher order–image photons contribute nonnegligibly to the observed line intensity. Our calculations show that the first-order–image line can contribute as much as 80% or even more of the zero-order–image line intensity to the observed line for a highly inclined disk.

Subject headings: accretion, accretion disks — black hole physics — galaxies: active — gravitational lensing — relativity

1. INTRODUCTION

Features of the emission lines of active galactic nuclei (AGNs) and Galactic black hole candidates are considered to be an important signature of the accreting matter around a black hole, although such other models as binary systems or jets can also produce similar features sometimes as predicted by disks. Broad double-horned line profiles have been resolved in the optical spectra of several AGNs, and the profiles have been well fitted with those from accretion disks around black holes, for example, the Balmer lines of Arp 102B, 3C 332 (Halpern 1990; Chen, Halpern, & Filippenko 1989). The two horns are due to the blueshift and redshift of light as the accreting matter moves toward and recedes from us. The big "UV bump" in the ultraviolet emission of Seyfert 1 galaxies or quasars, and the double-peaked optical lines constitute a proof of an accretion disk extending at least up to $10^3\ r_S$ (where r_S is the Schwarzschild radius $r_S = 2GM/c^2$). The iron line at 6–7 keV, originating from the innermost part of an accretion disk, has also been detected in the X-ray spectra of some AGNs (>90% of Seyfert galaxies) and Galactic black hole candidates (Barr, White, & Page 1985; White et al. 1986; Pounds et al. 1989; Nandra et al. 1989; Pounds et al. 1990). The discovery of high-energy spectra flattenings (the "hard tail" above ~10 keV) together with the iron K fluorescence line are currently interpreted as due to cold "reflecting" matter ($<10^7$ K) around a black hole, although the detailed structure of the profile remains unresolved due to the poor energy resolution of current X-ray satellites.

The study of the emission line would eventually enable us to map the innermost region of active galactic nuclei. X-ray profiles can differ, in some cases, a great deal from double-horned profiles due to the strong influence of the gravitational field around a black hole. By far, there has been extensive study of the iron line using full relativistic treatment (Fabian et al. 1989; Stella 1990; Laor 1991; Kojima 1991; Chen & Eardley 1992; Bao 1993; Matt et al. 1993 and references therein). However, an important factor both to the shape of the line and to its strength has been ignored throughout, namely, the contribution of higher order images of the disk (hereafter we adopt the definition of Cunningham & Bardeen 1973, i.e., the order of an image is equal to the number of times the photon crosses the equatorial plane). It has always been taken for granted that only the photons coming directly from the emitting material (the zero-order image) are important, whereas the higher order images can be neglected due to their faintness and also to the supposition that they are absorbed by the disk, anyway. However, this conviction has never been verified.

Quantitative studies of the effects of multiple imaging on the light curve and the image of the orbiting object around a black hole been undertaken by using quasi-analytic solutions of photon geodesics (Bao, Hadrava, & Østgaard 1994, hereafter Paper I), where it is shown that due to the lensing effect, the flux of higher order images of an emitting source around a black hole can in some orbital phases reach a value as high as, or even higher than the zero-order image. The role of the higher order images has also been discussed recently by Viergutz (1993), who claims that the back side of an accretion disk in many cases also exposes itself to the observer due to the

[1] Physics Institute, University of Trondheim, AVH, N-7055 Dragvoll, Norway.
[2] E-mail: bao.gang@avh.unit.no
[3] Astronomical Institute of the Academy of Sciences of the Czech Republic, CS-251 65 Ondřejov, Czech Republic.
E-mail: had@suhstel.asu.cas.cz
[4] E-mail: erlend.oestgaard@avh.unit.no

gravitational bending of light when the disk's inclination is very high. It is clear from the symmetry that for a disk viewed exactly edge-on the radiation from each side of the disk contributes to the observed signal just 50% of the total flux!

A disk may also be optically thin, which offers opportunities of higher order photons to reach the observer. First, the disk can be "clumpy" (Fabian 1990; Fabian & George 1991; Day et al. 1990), i.e., consisting of many clouds, with each one being optically thick to be responsible for the observed line emission, but sufficiently small, leaving the disk plane transparent. This scenario is supported by the short-term X-ray variability of AGNs (Abramowicz et al. 1991; Wiita et al. 1991; Bao & Østgaard 1994). Second, for a smooth disk, a photon emitted in a line will be, in general, gravitationally and Doppler-shifted with respect to the local flow in the crossed disk. It is obvious (see, e.g., [A2]) that this shift is determined by the radii of the events of emission and of the crossing point in the disk plane and that the relative value of the shift is of the order of the difference of ratios r_S/r for these radii; hence, in the inner parts of the disk, it is generally far larger than the width of the line. The probability of penetration of the line photon through the disk will thus be limited only by the lower opacity in the continuum. Moreover, the temperature and ionization in the innermost region of the disk can be expected to be so high (see, e.g., Wandel & Liang 1991; Collin-Souffrin 1992) that the electron scattering will dominate the opacity and might open an optically thin "central window." Finally, the Keplerian motion turns into free fall below the marginally stable circular orbit at $r = 6M$, and its radial component reaches the value of several tenths of the light velocity c. The column density of the disk and its optical thickness thus decreases significantly at least in this dynamic region. The latter can be estimated as $\tau \sim (\sigma c/mG)(\dot{M}/M)$ or $\tau \sim 30\ L/L_{\rm Edd}$ for a disk around an extreme Kerr black hole and $\tau \sim 200\ L/L_{\rm Edd}$ for a disk around a Schwarzschild black hole, where M is the mass of the black hole, $\dot{M}$ is the accretion rate, σ is the electron cross section, m is the mass of a hydrogen atom, and L and $L_{\rm Edd}$ are the luminosity of the source and the Eddington luminosity. Even if the conditions of the disk to be transparent are quite strict, i.e., the disk must be either very clumpy or, if smooth, then the mass rate must be highly subcritical to let $\tau < 1$, their possible observable consequences are still worthy of investigation.

In this paper, we extend our previous work by considering the contribution of higher order images to the emission line from an accretion disk around a Schwarzschild black hole and show the role of the higher order–image photons. Here we assume the disk to be completely transparent at least in some central region. The most realistic as well as the most complicated case of $\tau \sim 1$ will be studied elsewhere.

After the introduction, in § 2, both the method and the model used in the present work are described. Numerical results are shown in § 3. In § 4, the results are summarized and their astrophysical implications are discussed.

2. MODEL AND METHOD

The technique for calculating photon trajectories and the intensity of the images of a part of a disk has already been described in Bao (1992) and Paper I. Here we adopt the same quasi-analytic method. Physical quantities such as flux, photon arrival time, etc. are expressed in terms of a single parameter B, i.e., the total impact parameter. B is derived by solving geometric relations (expressed through elliptic integrals) for a null geodesic connecting with the observer at infinity. Figure 1

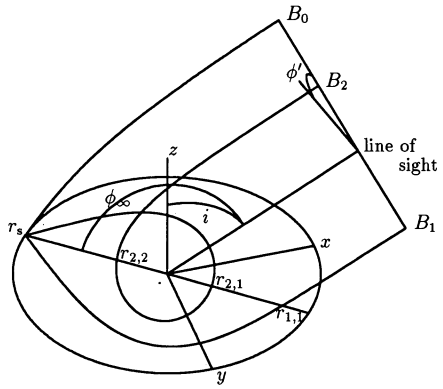

FIG. 1.—Photon trajectories close to a black hole. B_n refers to the impact parameter for a photon with nth order image, $r_{n,i}$ refers to the radius of crossing times, i, of the nth-order image photon. The r_S is the orbital radius of emitting matter.

describes the geometry considered. In the following part, we give a general description of the model and show some additional formulae which have not been covered in Paper I, but for the sake of convenience, the relevant formulae will be summarized in Appendix A.

For simplicity, we assume that line photons escape freely to us once emitted. This means that the corona around the emitting matter is optically thin. The emission line is emitted from a geometrically thin accretion disk with an inner radius r_i and an outer radius r_o in an equatorial plane of a black hole. Its presence may be attributed to the internally generated radiation or to the reprocessing hard X-ray photons. Here we only consider the Doppler broadening of line due to the relativistic rotation of the accreting matter, neglecting such mechanisms as thermal broadening and Compton broadening. The rest energy of the line emitted is E_0, and the specific line intensity $I_{\rm em}$ is the comoving frame of the emitting matter is approximated as a delta function:

$$I_{\rm em} = \epsilon(r, \mu)\delta(E_{\rm em} - E_0) \text{ ergs cm}^{-2} \text{ s}^{-1} \text{ Hz}^{-1} \text{ sr}^{-1},$$

where $\epsilon(r, \mu)$ is the emissivity of the line, depending on the radius from the center and the cosine of the emission angle (the angle between the direction of emission and the normal to the disk). It is well known that for a narrow beam of photons (e.g., Misner, Thorn, & Wheeler 1973),

$$\frac{I_\nu}{\nu^3} = \text{const}$$

along the photon trajectory. So the total flux of the line observed is

$$F = \int \epsilon(r, \mu) g^4 d\Pi \text{ ergs s}^{-1},$$

where $g = E/E_0$ and Π is the solid angle of the emitting matter subtended at the observer.

For an iron line, its emissivity $\epsilon(r, \mu)$ is subject to the radiation of the hard X-ray source (determined by its physics and geometry) and to the detailed physics of its reprocessing by the emitting material, i.e., to the structure of the disk. Here we follow the traditional simplification (e.g., Fabian et al. 1989) taking the dependence on the radius as a power law,

$$\epsilon(r, \mu) \sim f(\mu) r^\alpha,$$

assuming

$$f(\mu) = (1 + a\mu)\mu^b ,$$

where $\mu = \cos \hat{\theta}$. The emission angle $\hat{\theta}$ is measured in the comoving frame of the emitting matter (see Appendix A). Different values of coefficients a and b correspond to different local conditions of emitting matter, for example, $a = 0$, $b = 0$ for the case where the line emission is from optically thick matter; $a = 0$, $b = -1$ for the optically thin case; and $a \neq 0$, $b = 0$ for a general "limb-darkening law" (see, e.g., Chen & Eardley 1991; Matt, Perola, & Stella 1993).

The geometry of the inner accretion disk surrounding a black hole is poorly understood and the relevant optical thickness is unknown. We assume here that there is a critical radius r_c, characteristic of each disk, below which the disk is optically thin and above which it is opaque for the photons in question. It is thus decided for each ray of higher order image if it crosses the disk plane at the central window $r < r_c$ or if the photons are absorbed by the disk. We call this screen effect.

The nth-order ray will cross the equatorial plane n times, but the radius of the last crossing is the largest one. There is no turning point between the last crossing and the observer (see Appendix B). This knowledge enables us to avoid the calculation of each crossing of the trajectory with the equatorial plane and to utilize the expressions for the photon path in terms of elliptic integrals. We have thus the formula for calculating the radius r_{LC} of the last crossing.

$$n\pi = 2\left(\frac{p}{q}\right)^{1/2}\left\{F\left[\frac{\chi(r = r_{LC})}{2}, k\right] - F\left[\frac{\chi(r = \infty)}{2}, k\right]\right\},$$

(see Appendix A for details).

3. NUMERICAL RESULTS

To understand the detailed structure, we first calculate the line profile from a tiny ring at $r = 10r_s$ and $i = 85°$. Figure 2 gives the line profiles (see the second and the third rows); the relation of flux F and redshift g of the line in the first row in the course of the orbital motion of a disk element. The columns represent (left to right) the profiles of zero, the first, the second, and the third images. Line profiles in the third row exclude all the photons whose trajectories cross the accretion disk beyond $r = r_c = 10r_S$, while those in the second row include the contribution of all photons; profiles in both cases are normalized to their maxima. The shape of the line profiles depends on the relation $F(g)$ and on the time dt/dg spent by the image of the disk element in an interval of g. The zero-order profile clearly shows four peaks: the first and the fourth correspond to the extremal values of the radial velocity, where g varies slowly; the second and the third are due to gravitational lensing when the emitting matter is behind the black hole—the central

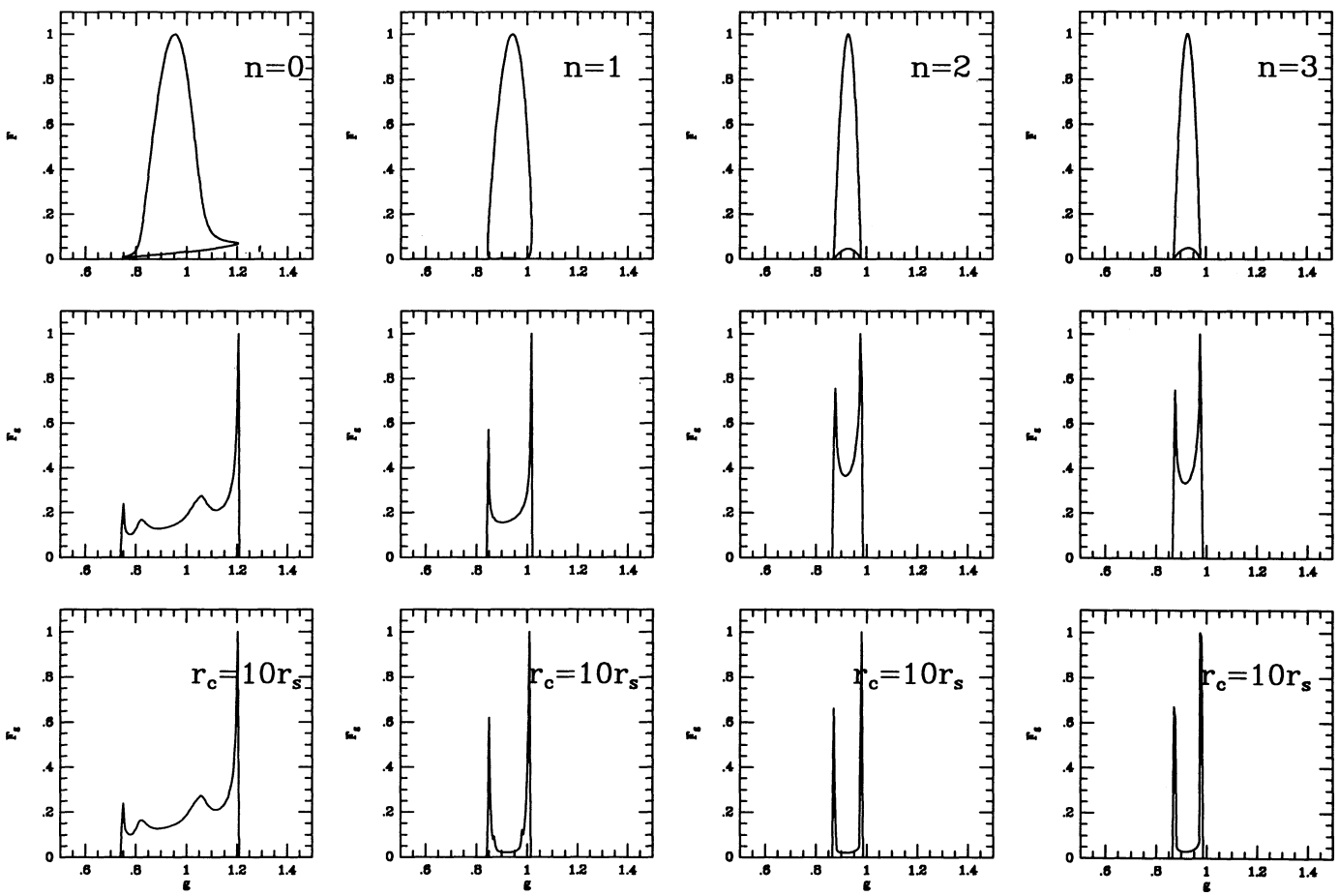

FIG. 2.—Line profiles (the second and the third rows) of different orders of image (the n in each column) and the F-g relations (between flux F and redshift g, the first row) for a ring at $r = 10r_S$ viewed at inclination $i = 85°$, where $g = E/E_0$, i.e., the ratio between energy of line and its rest value. Line profiles in the third row exclude all the photons whose trajectories cross an accretion disk beyond $r = r_c = 10r_S$, while those in the second row include the contributions of all photons.

TABLE 1

ENERGY RATIOS AMONG DIFFERENT ORDERS OF LINES: $r = 10r_S$

i (1)	$n = 0$ (2)	$n = 1$ (3)	$n = 2$ (4)	$n = 3$ (5)	$n = 4$ (6)
89°.5.....	1.000	0.7853	8.2164×10^{-3}	3.3057×10^{-4}	1.4299×10^{-5}
85	1.000	0.2789	3.4149×10^{-3}	1.3919×10^{-4}	6.0220×10^{-6}

depression is a result of the fast change of g at the maximum of the brightening. These features caused by lensing will disappear when the inclination i is small. We can see from the second row of the figure that there are no more than four peaks in the line profile of zero order. This feature has been discovered earlier by Bao & Stuchlík (1992), Bao (1993), and Matt et al. (1992, 1993). Although there are two peaks in the light curve (Paper I) of the first-order image, the corresponding maxima of $F(g)$ are seen at the same value of g. Therefore, the two peaks in the light curve have not given rise to a feature more complicated than the zero order. The F-g diagram shows closed curves for a closed ring; the upper part of the flux corresponds to the contribution from the half-ring on the side away from the observer, whereas the lower part corresponds to the contribution from the other half ring on the side close to the observer. The screening effect does not change much the shape of the line profile, but reduces its strength. In these cases, the photons emitted from the side away from the observer are hidden by the screening (see also Fig. 1). The ratios of the total intensity of the line for different orders to the zero-order line are given in Table 1. The first column gives inclination angle i, and columns (2)–(6) correspond to different orders of the image. We see that for the given conditions, the total intensity of the first-order image reaches $\sim 80\%$ of the zero order. The values of the line intensities for the higher order images decrease exponentially when $n \gg 1$, e.g., $F_4/F_3 \sim 0.0433 \sim e^{-\pi}$ (see Appendix A for an analytic proof). The lines corresponding to the higher order images are generally narrower, as the corresponding photons are emitted almost toward the center to reach the observer. After several orbits around the black hole, the direction of the photon emission is almost perpendicular to the orbital velocity of the disk; hence, the Doppler effect has a negligible influence on g, and there is only a gravitational redshift of the line.

Figure 3 shows the line profiles from a disk. Each row corresponds to the same labeled inclination angle, and each column

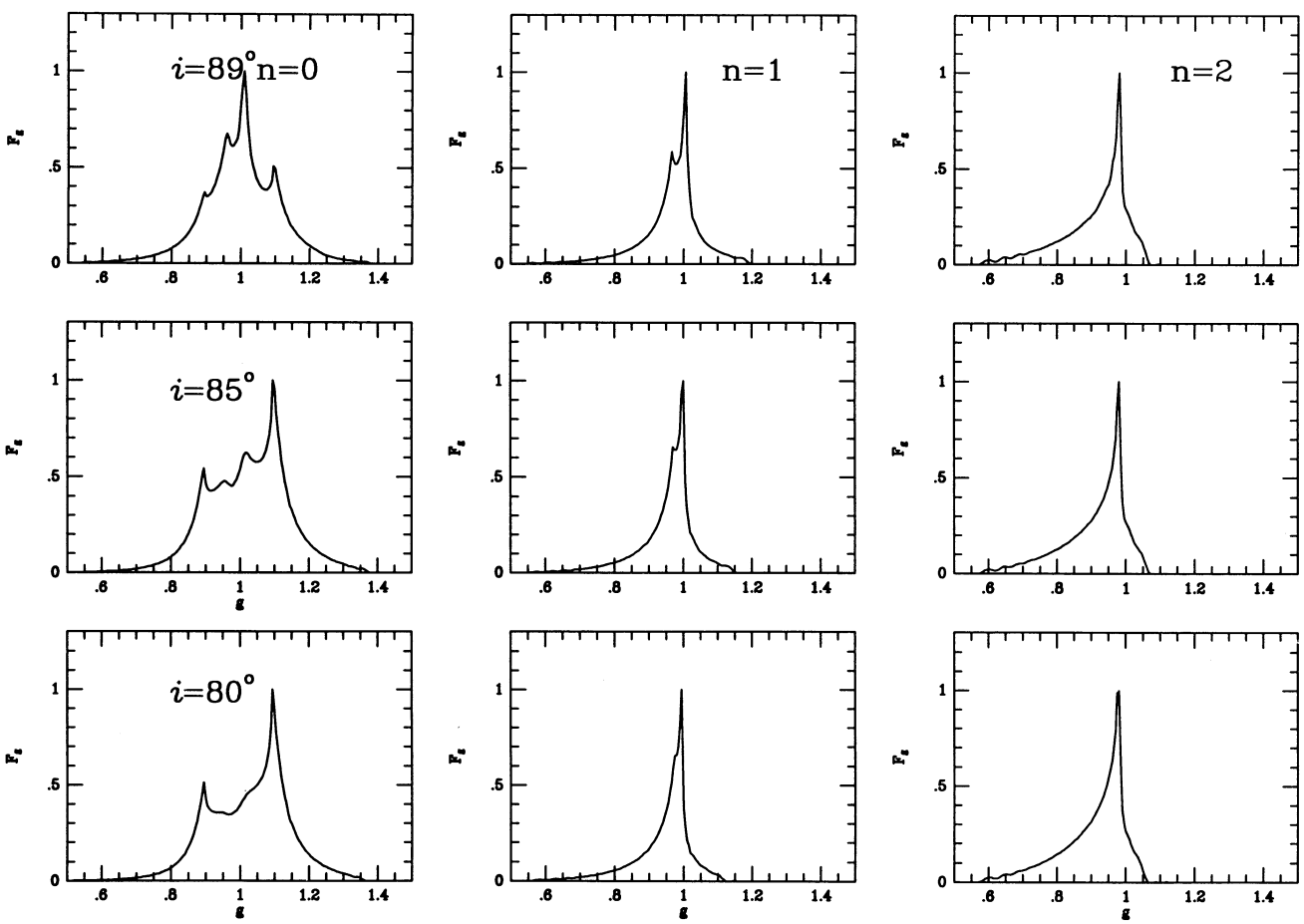

FIG. 3.—Line profiles for isotropic radiation from $r_i = 3.5r_S$ to $r_o = 50r_S$, with the index of line emissivity $\alpha = -1$. Each row corresponds to the same labeled inclination angle, and each column to the same order of image. $f(\mu)$ is taken to be a constant.

TABLE 2

ENERGY RATIOS AMONG DIFFERENT ORDERS OF LINES: $r_i = 3.5r_S$, $r_o = 50r_S$

i	$n = 0$	$n = 1$	$n = 2$
80°	1.00	0.05	4×10^{-4}
85	1.00	0.12	8×10^{-4}
89	1.00	0.48	8.8×10^{-2}
89.5	1.00	0.65	1.13×10^{-1}

TABLE 3

ENERGY RATIOS AMONG DIFFERENT ORDERS OF LINES: $r_i = 3.5r_S$, $r_o = 25r_S$, $\alpha = 0$

i	$n = 0$	$n = 1$	$n = 2$
80°	1.00	0.06	4×10^{-4}
85	1.00	0.15	1×10^{-3}
89	1.00	0.52	2×10^{-3}
89.5	1.00	0.68	2.5×10^{-3}

corresponds to the same order of image. Line emission is considered from $r_i = 3.5r_S$ to $r_o = 50r_S$, and the index of emissivity of the line is $\alpha = -1$. For an easy comparison of the profiles corresponding to different orders, we plot (in the first column) the line profiles of the zero-order image, which has already been shown by many authors. The line profiles of zero order for high inclination show more features due to gravitational lensing. The multipeaked feature disappears from the higher order images, because the blue horns are always higher than the red ones, and, in the summation of the contributions from the different rings of the disk, the red ones are too small to be seen in the profile. Note that the single peak in the higher order–image line is always redshifted by a small value. The line with the rest energy of 6.4 keV is shifted to the red for ~ 0.13 keV. The ratios of the total intensities of the higher order lines to the zero order are given in Table 2. The larger the inclination i is, the more the higher order image contributes. For $i = 89°.5$, the intensity of the first order is 65% of the zero order.

Figure 4 gives line profiles for a narrower range of a disk with $r_i = 3.5r_S$, $r_o = 25r_S$, and the emissivity coefficient $\alpha = 0$, $a = 0$, and $b = 0$. The corresponding energy ratios to the zero order are given in Table 3. The first-order lines are marked by double horns, with the blue horn being close to the rest energy of the line and always higher than the red one. The energy ratio of the first-order line to that of zero order reaches 68% for $i = 89°.5$. Note that the gradient of the ratios is large when i is approaching 90° (for $\Delta i = 0°.5$, the difference of the ratio between $i = 89°$ and $i = 89°.5$ is 0.13!). We expect that when $i = 90°$, the energy ratio of the first-order line to that of zero order could be 100%, as the two sides of the disk contribute equally to the total flux.

We have also examined the line profiles for nonisotropic radiation in the comoving frame. Figure 5 shows the line

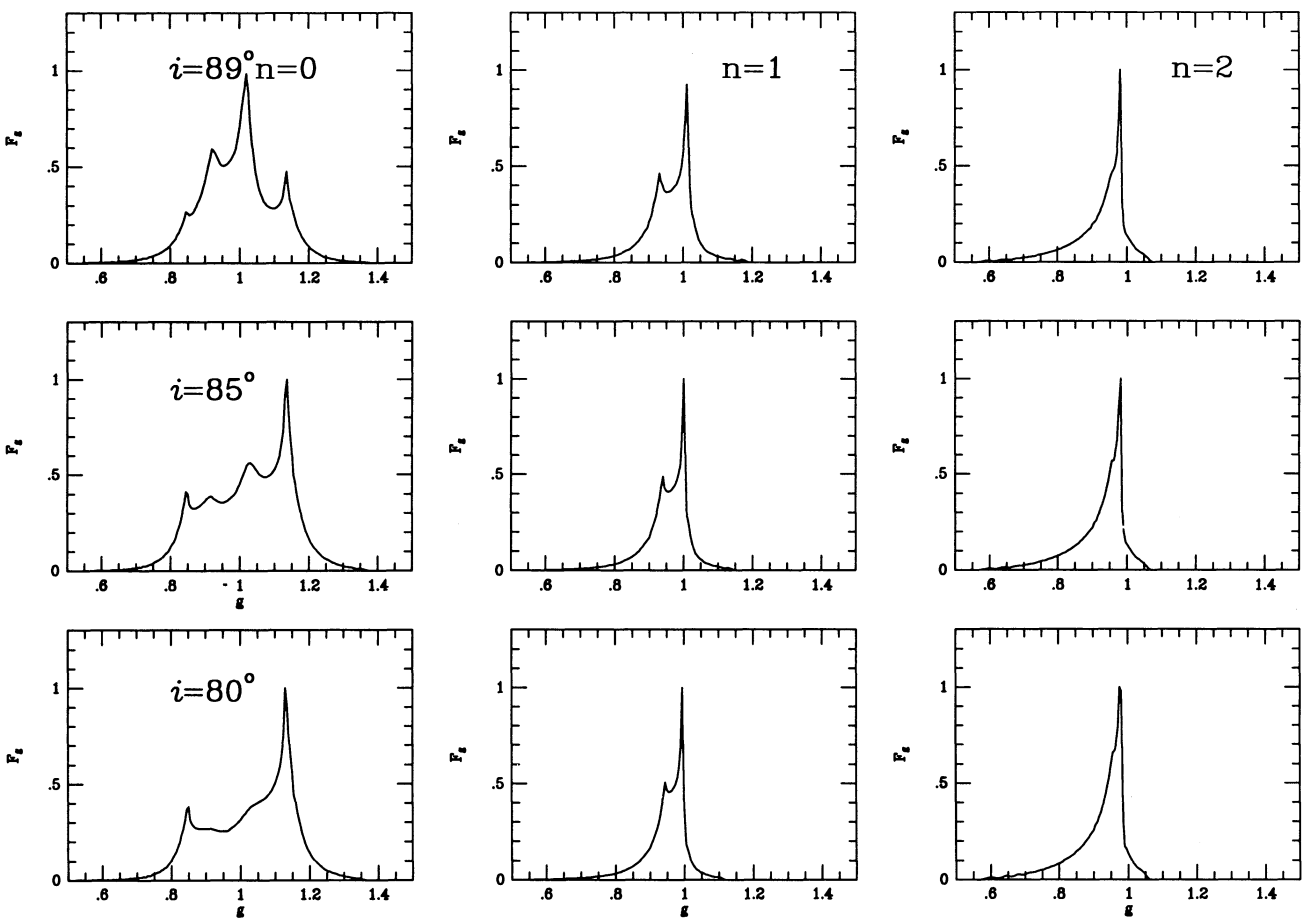

FIG. 4.—Line profiles for isotropic radiation from $r_i = 3.5r_S$ to $r_o = 25r_S$ with the index of line emissivity $\alpha = 0$. Each row corresponds to the same labeled inclination angle, and each column to the same order of image. $f(\mu)$ is taken to be a constant.

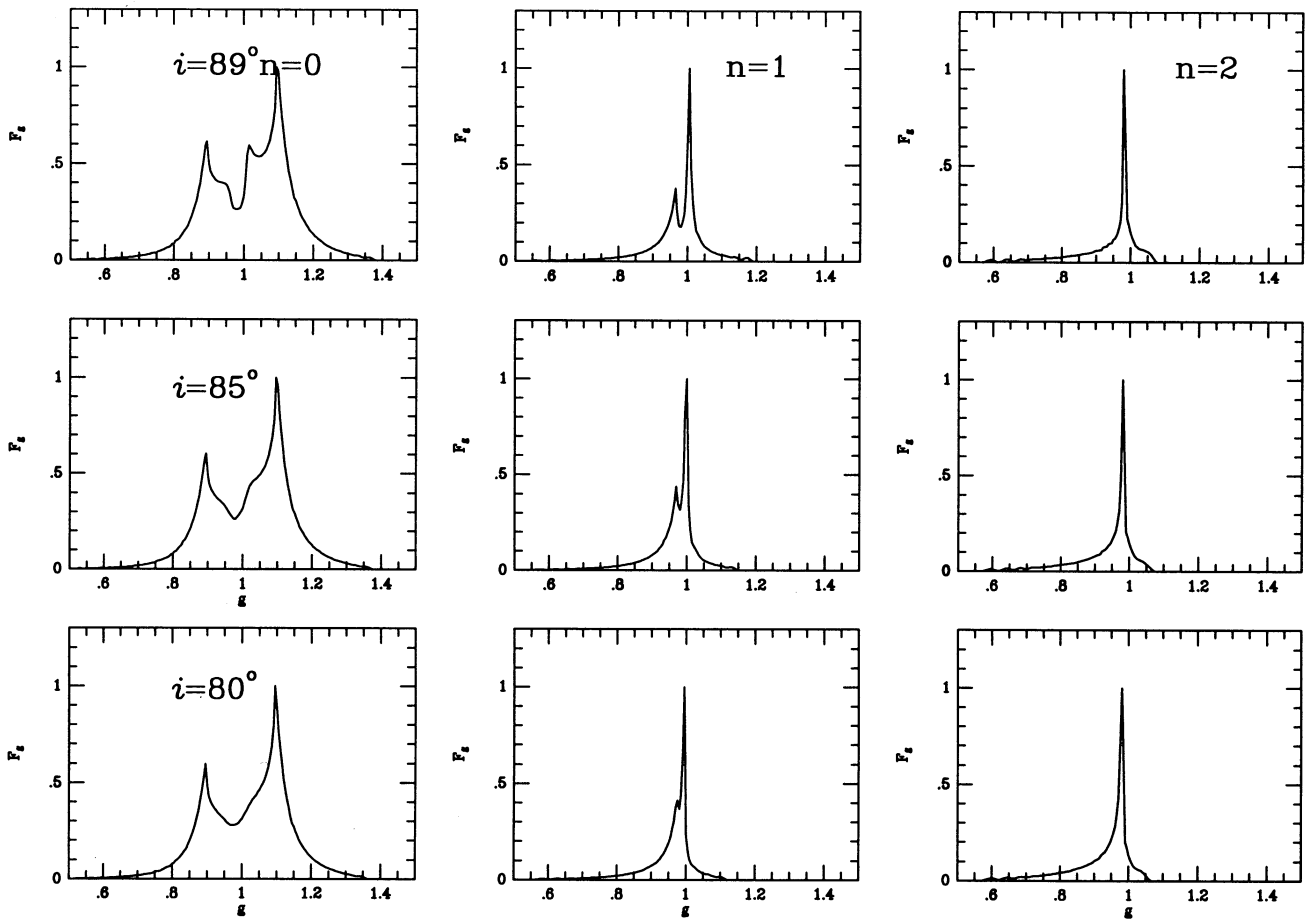

FIG. 5.—Line profiles for nonisotropic radiation from $r_i = 3.5r_S$ to $r_o = 50r_S$ with the index of emissivity of line $\alpha = -1$. Each row corresponds to the same labeled inclination angle, and each column to the same order of image. $f(\mu)$ is taken to be $\sim 1/\mu$.

profile for $f(\mu) = 1/\mu (a = 0, b = -1)$ from a disk with $r_i = 3.5$ and $r_o = 50r_S$, with the line emissivity index $\alpha = -1$. The total intensity ratios of the lines of different orders to those of zero order are given in Table 4. The shape of a zero-order line is also multi-peaked, but the peaks due to gravitational lensing are not as prominent as in the case of isotropic radiation. A double-horned line appears when the inclination satisfies $i \leq 85°$, while in the case of isotropic radiation, the double-peaked line profile appears only when $i \leq 80°$. Apart from the tiny double peaks at the top of the first-order lines, no important difference has been seen between higher order lines of $f(u) = 1/u$ and those of $f(u) = \text{const}$. The intensity ratios are also less prominent (see Table 3).

The cases of $a = 2.06$, $b = 0$ have also been calculated. The line profiles are similar to those for $a = b = 0$.

TABLE 4

ENERGY RATIOS AMONG DIFFERENT ORDERS OF LINES: $r_i = 3.5r_S$, $r_o = 50r_S$, $f(\mu) \sim 1/\mu$

i	$n = 0$	$n = 1$	$n = 2$
80°	1.00	0.05	5×10^{-4}
85	1.00	0.07	6×10^{-4}
89	1.00	0.13	9×10^{-4}
89.5	1.00	0.16	1×10^{-3}

Finally, we screen the disk by $r_c = 15r_S$. Its physical underpinning will be discussed later. In many cases, the screened line intensity is small, and the line profiles are not different from those shown. Here are the results of several cases: for $\alpha = -3$, $r_i = 3.5r_S$, $r_o = 25r_S$, the energy contribution due to the first-order line is 6% of its zero order for $i = 85°$, 7.7% for $i = 80°$, and 8.5% for $i = 75°$. The fact that the first-order line contribution increases as the inclination decreases arises from the trajectories of first-order photons that have smaller r_{lc} for smaller inclination, thus having more chances to penetrate the region below r_c.

4. DISCUSSION AND CONCLUSIONS

4.1. *Summary of the Results*

Using quasi-analytical method, we have calculated emission-line profiles for the disk images of various orders and have shown profiles with different parameters. The main conclusions are as follows:

1. The contribution of the higher order–image photons to the total intensity of the line is not negligible for an optically thin (e.g., clumpy) disk, particularly when the disk has a higher inclination angle, in which case it can count as much as ~40% or even more of the total intensity (Table 1). The first order is important, others decaying exponentially.

2. The fine structure of the zero-order lines of highly inclined disks due to relativistic effects is significantly influenced by the first-order contribution, which has smaller width. The profile of a combined line is thus subject to the inclination of the disk. For inclination $i < 80°$, the intensity ratio of the higher order–image line to the zero-order line is small, and the structure of the latter is dominant: the profile is double-horned. For high inclination, the fine structure of the total line is distorted much by the structure of the higher order–image line which, depending on the distribution of disk brightness, tends to form a single peak close to the rest energy, but a little bit redshifted. For an iron line at 6.4 keV, this peak will be shifted to the red by a value of ~ 0.13 keV.

3. Less pronounced by qualitatively the same results are valid for optically thick (smooth disks with transparent central windows. For éxtremely inclined disks with outer radii which are not much extended and vertical structure of optically thick part, the first-order photons with the last crossing points, r_{1c}, much larger than the outer border of an accretion disk can also contribute to the line.

4. The results reported in this paper are suitable for the lines radiated within the scale of several Schwarzschild radii from the central black hole such as the iron fluorescence lines observed in AGNs and X-ray binaries. They could also be applicable to the optical lines considered to originate from the inner part of an accretion disk (Halpern 1990).

4.2. *Possible Astrophysical Implications*

The visibility of the higher order images is constrained by several geometric and physical conditions, the plausibility of which is not a priori clear. On the other hand, like the fine structure of the zero-order line profiles (see Matt et al. 1993), the first-order contribution should leave its characteristic traces in the total line profile. The shape of the line gives an important clue to the mapping of the emission region. Hopefully, the next generation of X-ray satellites will resolve the fine structure of the iron line. This yields a chance to identify the possible contribution of the higher order image and to obtain both local and global information on the source. If the signatures of higher order lines were detected, this would have implications on the unification models of AGNs, as it suggests a high inclination of the source; also one may deduce that the source may be a very sub-Eddington one, or its emission region is very clumpy. Seyfert 1 nucleus of Mrk 841 was reported by Day et al. (1990) to show a strong iron line with an equivalent width of about 400 eV, which cannot be simply explained by the "reflection" model, although one cannot rule out an increased iron abundance for Mrk 841 in isolation. A plausible model of Mrk 841, as suggested, is that the accretion disk may be "clumpy." If this were the case, then the higher order line would contribute to the observed structure of line.

The effect of the higher order image is increasing with the inclination; hence, it can be observable only for sources with i higher than, $\sim 85°$, i.e. for about 10% of sources with randomly distributed axes. For a much smaller part of highly inclined disks with opaque outer region, the self-eclipse of the first-order image (but partially also the zero-order one; Bao 1993) can take place, depending on the geometry (both the radial and vertically extents) of the region.

The reflection models, i.e., reflective slab, accretion disk (e.g., George & Fabian 1991; Matt et al. 1992), are viewed as capable of explaining the higher energy flattening ("hard tail") and the fluorescent iron line phenomenon of AGNs. Hard X-rays are reprocessed into fluorescent emission, and are "reflected" by the cold accreting materials. The geometry of the cold "reflecting" matter is still poorly known, except for a few cases. In a fitting to NGC 5548, Nandra et al. (1992) concluded that the reflecting matter may range from $15r_S$ and further out. We have screened the disk by a value of $15r_S$. The contribution from the higher order images of the photons is still a sizable value. The first order can still account for $\sim 10\%$ of its zero order for a wide range of inclination. As can be seen from Figure 2, the screen effect does not affect the basic shape of the lines; therefore the line profiles shown are representative.

G. B. thanks M. Rees and M. Abramowicz for the discussions during the Copenhagen Hot Spot Conference, 1993 April. The authors are also indebted to the referee for his constructive suggestion. This work is supported by The Norwegian Research Council and by the grant Nr. 202/93/0503 from the Czech Republic.

APPENDIX A

A1. FLUX OF LINE

The total flux of the line observed at infinity is

$$F = \int \epsilon(r, \mu) g^4 d\Pi \text{ ergs s}^{-1} , \tag{A1}$$

where g is the redshift factor,

$$g = \frac{\sqrt{(1 - v_s^2)[1 - (2/R)]}}{1 - \Omega L_z} , \tag{A2}$$

where

$$v_s = \frac{\Omega R}{\sqrt{1 - (2/R)}}$$

is the velocity of the spot measured in a local static frame, and

$$\Omega = \left(\frac{1}{R}\right)^{3/2}$$

is its angular velocity (hereafter, the spherical coordinate and the geometric units in which $G = c = 1$ will be used, and for simplicity, physical quantities are expressed as dimensionless ones). L_z is the projection of angular momentum of the photons with respect to the symmetry axis. Since photon motion is planar, L_z can be expressed in terms of the total impact parameter B,

$$L_z = B \sin i \sin \phi' , \tag{A3}$$

which is equivalent (to but formally simpler than) the analogous formula given by Bao (1992). Here i is the inclination angle of the disk (i.e., the angle between the symmetry axis and the line of sight), and ϕ' is the observed position angle of the emitting matter, which reads,

$$\sin \phi' = \frac{\sin \varphi_s}{\sqrt{1 - \cos^2 \varphi_s \sin^2 i}} . \tag{A4}$$

The solid angle $d\Pi$ is expressed in terms of the total impact of B,

$$d\Pi = \frac{B\, dB\, d\phi'}{d^2} , \tag{A5}$$

where d is the distance between the observer and the emitting matter. $d\Pi$ can be written in terms of the coordinates of the disk R and φ_s:

$$d\Pi = \frac{B}{d^2} \left| \frac{\partial(B, \phi')}{\partial(R, \varphi_s)} \right| dR\, d\varphi_s .$$

The Jacobian only contains $\partial B/\partial R$ and $\partial\phi'/\partial\varphi_s$ terms. $\partial\phi'/\partial\varphi_s$ is found to be

$$\frac{\partial\phi'}{\partial\varphi_s} = \frac{\cos i}{1 - \sin i^2 \cos \varphi_s^2} , \tag{A6}$$

and $\partial R/\partial B$ is

$$\frac{\partial R}{\partial B} = \frac{\sqrt{2u_s^2 - u_s^2 + B^{-2}}}{u_s^2 B^3} \int_0^{u_s} \frac{du}{\sqrt{(2u^3 - u^2 + B^{-2})^3}} , \tag{A7}$$

where $u_s = 1/R$. When there exists a periastron p on the trajectory of photon, $\partial R/\partial B$ can be expressed in terms of the first and the second elliptical integrals, $F(\chi/2, k)$ and $E(\chi/2, k)$

$$\frac{\partial R}{\partial B} = c_1 \left[a(\chi_r) - a(\chi_\infty) + 3k^2 \left\{ \left[F\left(\frac{\chi_R}{2}, k\right) - F\left(\frac{\chi_\infty}{2}, k\right) \right] b(k) + \left[E\left(\frac{\chi_R}{2}, k\right) - E\left(\frac{\chi_\infty}{2}, k\right) \right] c(k) \right\} + d(\chi_r, k) - d(\chi_\infty, k) \right] \text{ for T.P.} \tag{A7a}$$

and

$$\frac{\partial R}{\partial B} = c_1 \left[a(\chi_r) + a(\chi_\infty) - 3k^2 \left\{ 2K(k) - \left[F\left(\frac{\chi_R}{2}, k\right) - F\left(\frac{\chi_\infty}{2}, k\right) \right] b(k) - \left[2E(k) - E\left(\frac{\chi_R}{2}, k\right) - E\left(\frac{\chi_\infty}{2}, k\right) \right] c(k) \right\} + d(\chi_r, k) + d(\chi_\infty, k) \right] \text{ for n.T.P.} , \tag{A7b}$$

where

$$c_1 = 2\left(\frac{p}{q}\right)^{3/2} \left[\frac{4p}{(q - p + 6)}\right]^2 ,$$

$$a(\chi) = -\frac{2 \operatorname{ctg} \chi}{\Delta^3} ,$$

$$b(k) = \frac{2 - k^2}{3k^2 k'^2} ,$$

$$c(k) = \frac{2(2 - k^2)}{3k'^4} ,$$

and

$$d(k,\chi)=\frac{\sin\chi}{6k'^2\Delta}\left\{\left[k^2(3k^2-1)\sin^2\left(\frac{\chi}{2}\right)-3k^2+2-\frac{k^2(k^2+1)\sin^2(\chi/2)-2}{k'^2\Delta^2}\right]\right\},$$

(T.P. stands for turning point) with $K(k)$, $E(k)$ denoting the complete elliptic integrals of the first kind and the second kind and

$$q^2=(p-2)(p+6)\,,\qquad k^2=\frac{1}{2q}(q-p+6)\,,\qquad \sin^2\left(\frac{\chi_R}{2}\right)=\frac{4p/R+q-p+2}{q-p+6}\,,\qquad \sin^2\left(\frac{\chi_\infty}{2}\right)=\frac{q-p+2}{q-p+6}\,,$$

$$B^2=\frac{p^3}{p-2}\,,\qquad \Delta=\sqrt{1-k^2\sin^2\left(\frac{\chi}{2}\right)}\,,\qquad k'=\sqrt{1-k^2}\,. \tag{A7c}$$

A2. THE IMPACT PARAMETER B

The polar angle circumscribed by a photon in its orbital plane can be calculated from the geodesic equation:

$$\phi_\infty=\int_0^{u_s}\frac{du}{\sqrt{2u^3-u^2+B^{-2}}}\,. \tag{A8}$$

When the considered photon trajectory has a periastron, the formula can be expressed in terms of the Jacobian elliptic integrals in the form

$$\phi_\infty=\begin{cases}2\left(\frac{p}{q}\right)^{1/2}\left[F\left(\frac{\chi_R}{2},k\right)-F\left(\frac{\chi_\infty}{2},k\right)\right] & \text{T.P.}\,,\\ 2\left(\frac{p}{q}\right)^{1/2}\left[2K(k)-F\left(\frac{\chi_R}{2},k\right)-F\left(\frac{\chi_\infty}{2},k\right)\right] & \text{n.T.P.}\end{cases} \tag{A8a}$$

There is an infinite set of photon trajectories starting at the point R, φ_s and reaching an observer at the chosen inclination i. The trajectory crossing n times the line of sight is referred to as the nth-order image. From the geometry considered, one can find the angle of the direct (the 0th-order) image,

$$\cos\phi_{0,\infty}=\sin i\cos\varphi_s\,. \tag{A9}$$

For an nth-order image,

$$\phi_{n,\infty}=\pi\left(n+\frac{1-(-1)^n}{2}\right)+(-1)^n\phi_{0,\infty}\,. \tag{A10}$$

For a given observer (i is given) through equations (A8), (A8a), (A9), and (A10), one can solve the $B(\varphi_s, R)$ relation for each order of ray.

A3. THREE LOCAL DIRECTIONAL ANGLES

The three direction angles measured in a comoving frame of emitting matter can be expressed in terms of the total impact parameter B. They are

$$\cos\hat{\theta}=-\frac{p^{\hat{\theta}}}{p^{\hat{t}}}=\left(\frac{B}{r}\right)g\sqrt{1-\left(\frac{L_z}{B}\right)^2}=\sqrt{\left(1-\frac{2}{R}\right)(1-v_s^2)}\,\frac{[(B/R)^2-(L_z/R)^2]^{1/2}}{1-\Omega L_z}\,, \tag{A11}$$

$$\cos\hat{\gamma}=-\frac{p^{\hat{r}}}{p^{\hat{t}}}=\sqrt{\left(1-\frac{2}{R}\right)(1-v_s^2)}\,\frac{\{[1-(2/R)^{-1}-(B/R)^2\}^{1/2}}{1-\Omega L_z}\,, \tag{A12}$$

and

$$\cos\hat{\varphi}=-\frac{p^{\hat{\varphi}}}{p^{\hat{t}}}=\sqrt{\left(1-\frac{2}{R}\right)}\,\frac{\{\Omega R[1-(2/R)]^{-1}-(L_z/R)^2]^{1/2}\}}{1-\Omega L_z}\,, \tag{A13}$$

where $\cos\hat{\theta}$ is the angle between the normal of the disk and the direction of emission. p^θ, p^r, p^φ, and p^t are the components of four-momentum of a photon measured at the comoving frame of the matter.

Especially, if $R\to\infty$, then $B\to R\sin\phi_\infty$. Through equations (A3) and (A11), we have

$$\cos\hat{\theta}=\cos i\,.$$

A4. THE ESTIMATION OF HIGHER ORDER ENERGY

From equations (A8)–(A10), the angle $\phi_{n,\infty}$ for the nth -order image is related to its impact parameter B_n by the expression

$$\phi_{n,\infty}=\int\frac{du}{\sqrt{2u^3-u^2+B_n^{-2}}}\,.$$

Photons of very high orders of image perform most of their orbits around the black hole close to their periastra p, which are close to 3. If the periastron p_n of the nth-order image is written as

$$\frac{1}{p_n} = \frac{1}{3} - x_n \,, \tag{A14}$$

where $x_n \ll 1$, then, following equation (A7c),

$$B_n^{-2} = \tfrac{1}{27} - x_n^2(1 - 2x_n) \,. \tag{A15}$$

Using the substitution $u = \frac{1}{3} - x|_{x=x_n}^{1/3}$, the integral (A8) can be written as

$$\phi = \int [(1 - 2x)x^2 - (1 - 2x_n)x_n^2]^{-1/2} dx \,. \tag{A16}$$

The domain of this integration can be splitted as $\int = \int_{x_0}^{x_s} + 2\int_{x_n}^{x_0} + \int_{x_0}^{1/3}$, where $x_n \ll x_0 \ll 1$. Consequently,

$$\phi_{n,\infty} \simeq \int_{x_0}^{x_s} (1 - 2x)^{-1/2}/x \, dx + 2\int_{x_n}^{x_0} (x^2 - x_n^2)^{-1/2} dx + C' \simeq -2\ln|x + \sqrt{x^2 - x_n^2}| + C \,. \tag{A17}$$

Following equation (A10),

$$\pi n \simeq \phi_{n,\infty} \simeq 2\phi_{n,t} \simeq -2\ln|x_n| \,,$$

i.e.,

$$x_n \simeq \exp(-\pi n/2) \,. \tag{A18}$$

The Jacobian can be estimated for the asymptotic high orders from the condition

$$0 \equiv \frac{d\phi_{n,\infty}}{dB_n} = \frac{\partial\phi_{n,\infty}}{\partial x_s}\frac{dx_s}{dR}\frac{dR}{dB_n} + \frac{\partial\phi_{n,\infty}}{\partial x_n}\frac{dx_n}{dB_n} \simeq \frac{(1 - 2x_s)^{-1/2}}{x_s}\frac{1}{R^2}\frac{dR}{dB_n} + \frac{2}{x_n^2} B_n^{-3} \,;$$

hence

$$\frac{\partial R}{\partial B} \simeq 2.3^{-6}(R - 3)\sqrt{R(R + 6)}\, x_n^{-2} \tag{A19}$$

The specific intensity of the line of the nth order is then

$$F_{g,n} \sim \frac{\partial B}{\partial R} \sim x_n^2 \sim e^{-n\pi} \,, \tag{A20}$$

i.e., for $n \gg 1$, $F_{g,n}$ decreases exponentially and the contribution of all orders higher than a chosen n_0 can be estimated as a sum of geometric series (actually, the numerical results show that, say, in the case given in Table 1, the ratio of the third and the fourth order is consistent with the asymptotic ratio up to 3 digits).

APPENDIX B

The path of the ray of the nth order image of a source at radius $r_{\rm em}$ in the equatorial plane will cross n times the equatorial plane in radii $r_{n,i}$ and polar angles (measured in the plane of the photon motion) $\phi_{n,i}$, $i = 1, \ldots, n$. The point of emission can be identified with $i = 0$, the beginning of the polar axis can be chosen $\phi_{n,0} \equiv 0$, and the orientation in the direction of the motion of the photon. Crossings of the path may also occur with the equatorial plane in the opposite direction from the point of emission, labeled by the negative values of i. The ray then reaches the observer at infinity at polar angles $\phi_{n,\infty}$. The backward path of the ray can reach the infinity at angle $\phi_{n,-\infty}$.

LEMMA 1. *The radius of the last crossing is the largest one,*

$$\max(r_{n,i}|_{i=1}^{n}) = r_{n,n} \,.$$

LEMMA 2. *There is no turning point between the last crossing $\phi_{n,n}$ and infinity $\phi_{n,\infty}$ for $n > 0$.*

Proof. If there is no turning point on the path, the validity of both lemmas should be obvious. If there is a turning point at the polar angle $\phi_{n,t}$ then the path is symmetric with respect to this point, i.e.,

$$r(\phi_{n,t} + \phi) = r(\phi_{n,t} - \phi)$$

and clearly

$$\phi_{n,\infty} - \phi_{n,t} = \phi_{n,t} - \phi_{n,-\infty} > \phi_{n,t} \Rightarrow \phi_{n,t} < \tfrac{1}{2}\phi_{n,\infty} \,.$$

It is also obvious that $\phi_{n,k} = k\pi$ and $n\pi < \phi_{n,\infty} < (n+1)\pi$. Consequently,

$$\phi_{n,t} < \frac{1}{2}\,\phi_{n,\infty} < \frac{n+1}{2}\,\pi \leq n\pi = \phi_{n,n}\,,$$

whenever $n \geq 1$, which is the proof of the Lemma 2.

Further, $r_{n,n}$ at the last crossing is thus the largest on the uprising part ($\phi > \phi_{n,t}$) of the ray, while on its falling part (if $\phi_{n,t} > \pi$) it is the largest one $r_{n,1}$. However, $\phi_{n,1} - \phi_{n,-\infty} > \pi > \phi_{n,\infty} - \phi_{n,n}$; hence the first crossing is also deeper than the last one.

REFERENCES

Abramowicz, M., Bao, G., Lanza, A., & Zhang, X-H. 1991, A&A, 245, 454
Bao, G. 1992, A&A, 257, 594
———. 1993, ApJ, 409, L41
Bao, G., Hadrava, P., & Østgaard, E. 1994, ApJ, 425, 63 (Paper 1)
Bao, G., & Østgaard, E. 1994, ApJ, 422, L51
Bao, G., & Stuchlík, Z. 1992, ApJ, 400, 163
Barr, P., White, N. E., & Page, C. G. 1985, MNRAS, 216, 65P
Chen, K., & Eardley, D. 1991, ApJ, 382, 125
Chen, K., Halpern, J. P., & Filippenko, A. V. 1989, ApJ, 339, 742
Collin-Souffrin, S. 1992, in Testing the AGN Paradigm, ed. S. S. Holt, S. G. Neff, & C. M. Urry (AIP Conf. Proc. 254) (New York: AIP), 119
Cunningham C. T., & Bardeen, J. M. 1973, ApJ, 183, 237
Day, C. S. R., Fabian, A. C., George, I. M., & Kunidea, H. 1990, MNRAS, 247, 15P
Fabian, A. C. 1977, Nature, 269, 672
Fabian, A. C., & George, I. M. 1991, in Iron Line Diagnostics in X-Ray Sources, ed. A. Treves, G. C. Perola, & L. Stella (Berlin: Springer-Verlag), 169
Fabian, A. C., Rees, M., Stella, L., & White, N. E. 1989, MNRAS, 238, 729
George, I. M., & Fabian, A. C. 1991, MNRAS, 249, 352
Halpern, J. P. 1990, ApJ, 365, L51
Kojima, Y. 1991, MNRAS, 250, 629
Laor, A. 1991, ApJ, 376, 90
Matt, G., Perola, G. C., Piro, L., & Stella, L. 1992, A&A, 257, 63
Matt, G., Perola, G. C., & Stella, L. 1993, A&A, 267, 643
Misner, C. W., Thorne, K. S., & Wheeler, J. A. 1973, Gravitation (San Francisco: Freeman)
Nandra, K., Pounds, K. A., & Stewart, G. C. 1992, in Testing the AGN Pardigm, ed. S. S. Holt, S. G. Neff, & C. M. Urry (AIP Conf. Proc. 254) (New York: AIP), 163
Nandra, K., Pounds, K. A., Stewart, G. C., Fabian, A. C., & Rees, M. J. 1989, MNRAS, , 236, 39P
Pounds, K. A., Nandra, K., Stewart, G. C., George, I. M., & Fabian, A. C. 1990, Nature, 344, 132
Pounds, K. A., Nandra, K., Stewart, G. C., George, I. M., & Leighly, K. 1989, MNRAS, 240, 769
Stella, L. 1990, Nature, 344, 747
Viergutz, S. V. 1993, A&A, 272, 355
Wandel, A., & Liang, E. P. 1991, ApJ, 380, 84
White, N. E., Peacock, A., Hasinger, G., Mason, K. O., Manson, K. O., Manzo, G., Taylor B. G., & Branduardi-Raymont, G. 1986, MNRAS, 218, 129
Wiita, P. J., Miller, H. R., Carini, M. T., & Rosen, A. 1991, in IAU Colloq. 129, Structure and Emission Properties of Accretion Disks, ed. C. Bertout et al. (Gif-sur-Yvette: Editions Frontières), 557